Available online at www.sciencedirect.com
SCIENCE DIRECT®
Journal of Nuclear Materials 340 (2005) 125–148
journal of nuclear materials
www.elsevier.com/locate/jnucmat

RPV-1: A Virtual Test Reactor to simulate irradiation effects in light water reactor pressure vessel steels

Stéphanie Jumel *, Jean Claude Van-Duysen

EDF/R&D site des Renardières, Route des Renardieres, 77818 Moret sur Loing, France
Laboratoire de Physique et Génie des Matériaux (LMPGM), Université des Sciences et Technologies de Lille I, 56655 Villeneuve d'Ascq, France

Received 2 April 2004; accepted 11 October 2004

Abstract

Many key components in commercial nuclear reactors are subject to neutron irradiation which modifies their mechanical properties. So far, the prediction of the in-service behavior and the lifetime of these components has required irradiations in so-called 'Experimental Test Reactors'. This predominantly empirical approach can now be supplemented by the development of physically based computer tools to simulate irradiation effects numerically. The devising of such tools, also called Virtual Test Reactors (VTRs), started in the framework of the REVE Project (REactor for Virtual Experiments). This project is a joint effort among Europe, the United States and Japan aimed at building VTRs able to simulate irradiation effects in pressure vessel steels and internal structures of LWRs. The European team has already built a first VTR, called RPV-1, devised for pressure vessel steels. Its inputs and outputs are similar to those of experimental irradiation programs carried out to assess the in-service behavior of reactor pressure vessels. RPV-1 is made of five codes and two databases which are linked up so as to receive, treat and/or convey data. A user friendly Python interface eases the running of the simulations and the visualization of the results. RPV-1 is sensitive to its inputs (neutron spectrum, temperature,...) and provides results in conformity with experimental ones. The iterative improvement of RPV-1 has been started by the comparison of simulation results with the database of the IVAR experimental program led by the University of California Santa Barbara. These first successes led 40 European organizations to start developing RPV-2, an advanced version of RPV-1, as well as INTERN-1, a VTR devised to simulate irradiation effects in stainless steels, in a large effort (the PERFECT project) supported by the European Commission in the framework of the 6th Framework Program.

1. Introduction

Many key components in commercial nuclear reactors are subject to neutron irradiation which modifies their mechanical properties. So far, the prediction of the in-service behavior and the lifetime of these components has required surveillance programs, component

* Corresponding author. Tel.: +49 721 61 05 13 11/+33 6 14 40 01 21; fax: +49 721 61 05 13 32.
E-mail addresses: stephanie.jumel@edf.fr (S. Jumel), jean-claude.van-duysen@edf.fr (J.C. Van-Duysen).

0022-3115/$ - see front matter © 2004 Elsevier B.V. All rights reserved.
doi:10.1016/j.jnucmat.2004.10.131

sampling programs and irradiation programs in so-called 'Experimental Test Reactors'. For example, large-scale irradiation programs have been carried out in many countries to assess the end-of-life behavior of pressure vessel or internal structures of Light Water Reactors (LWRs), or to develop cladding materials for fuel elements. This predominantly empirical approach does not cover all the needs, mainly because some in-service conditions are almost impossible to reproduce with the existing test facilities. Moreover, it is also becoming more problematic because of the decreasing number of test reactors and post-irradiation characterization facilities. An increasing cost is also a serious drawback.

A proactive way to meet these issues is to develop physically based computer tools to simulate irradiation effects numerically. The development of such tools, also called Virtual Test Reactors (VTRs), is now accessible thanks to continuous progress in physical understanding of material degradation as well as in computer science and technology. It can take advantage of the larger and burgeoning field of computational material sciences. However, specific suites of multi-scale simulation codes have to be constructed by the irradiation effects community (e.g. [1,2]).

VTRs are not aimed at replacing Experimental Test Reactors but rather at complementing them. They can help perform design, safety and end of life analysis of nuclear installations in a very time- and cost-effective way. They can also be used for example: (i) to help design experimental programs, (ii) to explore conditions outside the existing experimental databases, (iii) to systematically evaluate the individual or combined influence of the material variables (composition and microstructure) and the service conditions (temperature, flux, spectrum, etc.) that may exceed the capacity of any experimental program, (iv) to help understand the phenomena leading to degradations, (v) to optimize the design and interpretation of irradiation surveillance programs, (vi) to support the training of young researchers in material science and radiation effects and (vii) to manage, consolidate and share the broad international knowledge production concerning irradiation effects. The VTRs also represent a key added-value for the global optimization of the irradiation and testing facilities which will be necessary in the coming decades.

The devising of VTRs started in the framework of the REVE Project (REactor for Virtual Experiments) and relies on previous efforts in modeling (e.g. [3,4]) and physically based data correlations carried out by the RPV community (e.g. [5]). The REVE project (e.g. [6–9]) is a joint effort between Europe, the United States and Japan aimed at building VTRs able to simulate irradiation effects in pressure vessel steels and internal structures of LWRs. The European team has already built a first VTR called RPV-1 devised for pressure vessel steels [6]. A part of the codes and data it uses, has been provided by the US and Japanese teams (led respectively by Professor R. Odette from UCSB and Dr N. Soneda from CRIEPI).

RPV-1 relies on many simplifications and approximations and has to be considered as a prototype aimed at clearing the way. Long-term efforts will be required to complete it and to build successive generations of more and more sophisticated versions. Nevertheless, RPV-1 can already be used for many applications (understanding of experimental results, assessment of effects of material and irradiation conditions...). Its inputs and outputs are similar to those of experimental irradiation programs carried out to assess the in-service behavior of reactor pressure vessels.

This article is the second of a series aimed at presenting the codes and models used to build RPV-1 [10,11]. Its objective is to describe the structure of the tool and to show its limits and potentialities. Section 2 gives a short survey of the knowledge concerning irradiation effects in RPV steels. Section 3 presents the models used in RPV-1 to simulate the formation of the irradiation-induced damage and the plasticity behavior in RPV steels. In Section 4, the architecture of RPV-1 as well as the codes implemented to build it are described; the successive simulation steps are also explained. Results of first simulations showing the sensitivity of RPV-1 to its input data are given in Section 5. The last section provides some elements about errors and uncertainties inherent to the approach adopted to build RPV-1.

A comprehensive comparison between results of simulations carried out with RPV-1 and results of experimental programs will be published in a companion paper [12].

2. Short survey on irradiation effects in RPV steels

RPV-1 relies on the current knowledge of irradiation effects in RPV steels which can be found in several comprehensive surveys (e.g. [13,14]). This section only reminds the main elements which are useful to understand how the simulations are carried out with RPV-1. It briefly shows the influence of the structure and chemistry of steels on their irradiation response. It also gives the current vision of their irradiation-induced damage and describes the mechanisms leading to this damage.

2.1. Influence of RPV steel parameters

2.1.1. Metallurgical structure

In principle, the microstructure plays a role in the irradiation-response of RPV steels in setting the types and quantities of sinks for point defects as well as in influencing the hardening by superposing the effect of

the pre-existing carbides to that of the irradiation-induced defects [14]. However, experimental studies and statistical analysis of experimental results show that, in the range of typical RPV steels, the irradiation response slightly depends on their structure (bainite, martensite, ...) and type (welds, forgings, plates) [15–17].

2.1.2. Chemical composition

The main results concerning the influence of alloying elements or impurities on RPV steel response to irradiation at about 290 °C can be summarized as following:

- *Copper* is one of the elements with the most deleterious effect (e.g. [18]). This effect appears at a copper content of about 0.04% (e.g. [19]) and becomes very strong above 0.1% [20]. Due to its low solubility limit at the irradiation temperature (≈0.007% in pure iron [21]) copper has a propensity to precipitate or to cluster in RPV steels under LWR irradiation conditions. Since the first model of the irradiation-induced embrittlement due to copper [3], a large literature has been treating the role of this element. (e.g. [4,21–26]).
- *Phosphorus* also has a significant deleterious effect when its concentration is higher than about 0.015%, due to its capacity to segregate into grain boundaries. The phenomenon reduces the cohesive energy of grain boundaries and may promote intergranular rupture initiation or propagation (e.g. [27]).
- *Nitrogen* has a low influence on the irradiation effect sensitivity of RPV steels at temperature over 250 °C. At a lower temperature, it may have a significant influence (e.g. [28,29]).
- *Nickel* has a strong deleterious impact on irradiation-induced embrittlement of RPV steels (e.g. [30–36]). This impact increases synergistically with the copper content and may become very high for nickel contents over about 1.1%. Experimental and/or thermodynamic studies (e.g. [14,37]) have shown that nickel can integrate copper-rich precipitates and clusters under LWR irradiation conditions. It may also be involved in nickel–manganese-rich phases containing a small amount of copper (late blooming phases [14]).
- *Manganese* has not been the object of dedicated experimental programs yet. However, as mentioned above, thermodynamic and experimental studies have shown that under irradiation manganese can integrate copper-rich precipitates and clusters. It may also participate in Ni–Mn-rich late blooming phases [14].

2.2. Nature of the irradiation-induced damage

Irradiation-induced embrittlement of RPV steels may stem from two types of damage: (i) an intergranular segregation of elements which may weaken the grain boundaries and (ii) an intragranular formation of defects which harden the grains (these defects are called 'hardening defects' in this document). Both of them have their origin in the so-called displacement cascades, resulting from the interactions between neutrons and lattice atoms. Before describing these two types of damage, let us remind some results on the role of displacement cascades.

2.2.1. Role of displacement cascades

The role played by displacement cascades in the neutron irradiation-induced embrittlement of RPV steels has been studied by experimental work and numerical simulation (Molecular Dynamics- and Binary Collision Approximation-type codes). Experimental work showed that the displacement cascades ease the nucleation of point defect clusters or loops as well as of vacancy-solute clusters in RPV steels [23,25,38,39]. Simulation studies (e.g. [40,41]) showed that neither the temperature (in the range 100–600 K), nor the substitutional alloying atoms (Mn, Ni, ...) or impurities (Cu, ...) significantly affect the ballistic and recombination phases (during some tens of ps) of displacement cascades in RPV steels (e.g. [41]). They neither influence their splitting into subcascades. It appeared also that the atomic re-arrangements produced by displacement cascades make a weak contribution to the irradiation-induced evolution of the RPV steel microstructure. It is the migration of some of the surviving point defects left by the cascades which is responsible for such an evolution. Indeed, by migrating, these defects interact with solute atoms and impurities, form clusters, are absorbed by grain boundaries, etc. All these phenomena lead to the nucleation and growth of hardening defects as well as to the segregation of elements to grain boundaries. It is noteworthy that under irradiation, the migration of solute atoms in RPV steels is much faster than under purely thermal conditions, because of the vacancy super-saturation (enhanced diffusion). Solute atoms may also interact with fluxes of SIAs or vacancies and hence migrate (induced diffusion) to sinks (grain boundaries, interfaces, ...) or hardening defects. For the induced diffusion, authors generally agree that phosphorus atoms are more strongly bound to SIAs than to vacancies (e.g. [42–45]). As for most of the other solutes atoms (Cu, Ni, ...), there is still a controversy.

2.2.2. Intergranular segregation

As already mentioned, phosphorus atoms can reach grain boundaries by random walk (enhanced segregation) or by following SIA fluxes (induced segregation). Boron and carbon atoms are also known as active segregants to grain boundaries. They enhance the cohesive strength of grain boundaries, and therefore reduce the degree of embrittlement due to the presence of phosphorus. It is also assumed that there is an atomic site

competition between boron, carbon and phosphorus atoms. Several models to forecast the degree of irradiation-induced segregation of phosphorus to grain boundaries are available (e.g. [46–48]). These models rely on slightly different sets of hypotheses and have been fitted against available data. They reproduce these data rather well but still need to be improved if they are to be used as reliable forecasting tools.

2.2.3. Hardening defects

Most of the experimental and simulation results showed that neutron irradiation induces the formation of four types of hardening defects in RPV steels:

- copper-rich precipitates also containing Mn, Ni and Si;
- vacancy-solute (Cu, Mn, Ni, Si) clusters;
- self-interstitial atom clusters (SIA clusters) and dislocation loops;
- vacancy clusters.

Experimental studies showed that the presence of copper is required for the formation of precipitates and vacancy-solute clusters (e.g. [38,39]). It was also noticed that some of the hardening defects are unstable (i.e. they have a lifetime [21,49]) at the RPV irradiation temperature (about 290 °C). They exist with a high number density thanks to a dynamical equilibrium state imposed by the irradiation.

2.2.3.1. Copper precipitates. Copper-rich precipitates were observed by High Resolution Electron Microscopy combined with Scanning Transmission Electron Microscopy in high copper iron-based alloys (e.g. [22]). Their existence was also indirectly proven by combinations of several characterization techniques (SANS, EXAFS,...) in low copper iron-based alloys. Thermodynamics-based calculations or simulations showed that they contain Mn, Ni and Si [37].

2.2.3.2. Vacancy-solute clusters. Solute atom clusters were clearly revealed by Atom Probe studies (e.g. [50–52]). They are composed of Cu, Mn, Ni, Si and Fe atoms. The threshold dose from which these defects are detected seems to decrease as the steel copper content increases (see Fig. 1 [13]). Whatever the fluence and steel chemical composition, their radius is lower than 2 nm and they mainly contain iron atoms. Composition profiles revealed that the manganese, nickel and silicon atoms seem to concentrate at the interface with the matrix [37,51]; their spatial extends are generally slightly larger than that of copper enrichment. Due to their low concentration in solute atoms (<20%, see review in [13]), the irradiation-induced solute atoms clusters are often called 'atmospheres' or 'clouds' [50]. The reason why such defects keep a dilute morphology and do not collapse in real precipitates is an issue which is still under discussion. A possible explanation may be the presence of a high concentration of vacancies within the defects. This explanation is at the origin of their name: vacancy-solute clusters. The existence of copper-vacancy cluster was first suggested by Odette [53] and is now supported by numerical simulation [54].

Experimental and simulation studies showed that, among the solute atoms in the clusters or precipitates, copper invariably has the highest enrichment factor over the matrix level. That explains the significant depletion of the copper content measured in the matrix; this

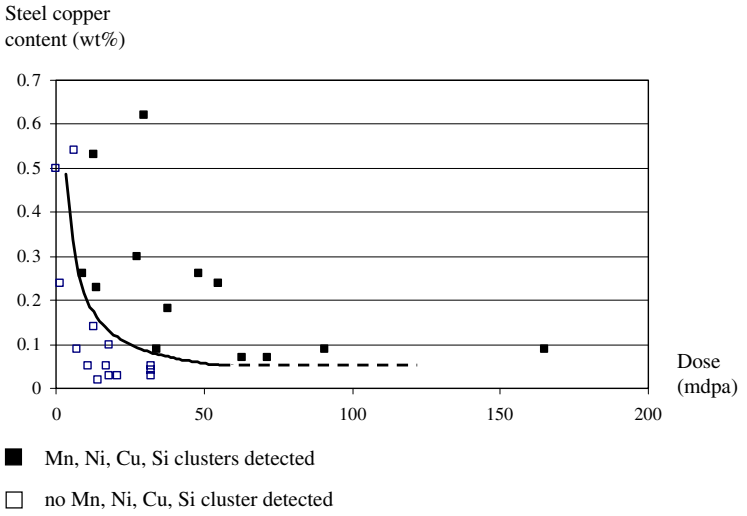

Fig. 1. Steel copper contents and doses for which Mn, Ni, Cu, Si clusters have been detected by Atom Probe experiments in irradiated RPV steels [13].

content tends to a lower limit of about 0.03–0.04% (e.g. [21]). For steels with a copper content of about 0.1–0.15 %, this limit is reached at a fluence of about 2×10^{23} n.m^{-2}. No significant depletion was measured for Ni, Mn and Si in the matrix.

The number density of vacancy-solute clusters increases with the copper and nickel contents of the steel as well as with the fluence. As an example, number densities of 3.3, 5.7 and 9×10^{17} cm^{-3} were measured with an Atom Probe in a 0.08%Cu steel irradiated at 275 °C with fluences of 2.5, 6.6 and 12×10^{23} n.m^{-2} ($E>1$ MeV), respectively (see a review in [13]).

2.2.3.3. SIA clusters and dislocation loops. The structure of SIA clusters is not completely understood yet. In particular, the set of properties that distinguishes SIA clusters and SIA dislocation loops is not well clarified [55–58]. According to Puigvi et al., and Kuramoto [55,57], about 160–200 SIAs are required for a cluster to behave fully as a dislocation loop; Wirth et al. (e.g. [56]) estimate that, except at very small size, both types of defect have analogous properties and can be considered as similar. To build RPV-1, we retained this latter position and assimilated SIA clusters to dislocation loops, what ever their size (of course for very small size it is an erroneous approximation). In the following, the terms 'loop' and 'cluster' will be equally used.

Loops are not observable in RPV steels neutron irradiated with nominal conditions of flux, fluence and temperature. However, TEM examinations of ferritic alloys irradiated with high doses ($\geqslant1$ dpa) (e.g. [59,60]) as well as MD simulations in Fe (e.g. [56,61–63,54]) showed that the stable SIA loops have for Burgers vector $b=\frac{1}{2}\langle111\rangle$ or $\langle100\rangle$ and for habit plan $\{111\}$ and $\{110\}$, respectively. Wirth et al. [56] described the $\frac{1}{2}\langle111\rangle$ loops as a mixture of $\langle111\rangle$ dumbbells and crowdions on $\{110\}$ planes, Soneda [61] and Osetsky [62] saw only the crowdions. Osetsky described the $\langle100\rangle$ loops as a set of $\langle100\rangle$ crowdions.

Simulation studies showed also that SIA clusters are mobile along $\langle111\rangle$ directions (e.g. [64–67]). They may switch their moving from a $\langle111\rangle$ direction to another one either by thermal activation or when they meet impurities, other SIA clusters, etc. Their migration is therefore achieved along a 3-D path made of 1-D segments (it is referred to as a mixed 1D/3D migration [66]). The capacity of clusters to switch their moving direction decreases with their size. The role played by SIA clusters and dislocation loops in the irradiation response of RPV steels is not yet well understood and quantified.

2.2.3.4. Vacancy clusters. Simulation studies showed that small vacancy clusters are more stable in a 3-D configuration than in a 2-D one [58,67]. However, it was also noticed that 3-D clusters containing more than about 30 vacancies may present some fragments of $\{110\}$ vacancy platelets, which mark the beginning of a loop nucleation [68,69]. Clusters containing more than about 100 vacancies may produce a stable nucleus of vacancy dislocation loop. Positron Annihilation studies confirmed the presence of vacancy clusters in irradiated iron-based alloys. They seem to be smaller in steels than in simple model alloys (Fe–Cu,...).

At around 290 °C, small vacancy clusters and dislocation loops have a 3-D and 1-D migration respectively [70]. They are much less mobile than SIA clusters and dislocation loops of similar sizes. Vacancy clusters are also much less mobile than vacancy loops. As for SIA's, the role played by vacancy clusters in the irradiation response of RPV steels is not yet well understood and quantified.

3. Models used to build RPV-1

A quantitative simulation of irradiation effects has to start by reproducing the primary events resulting from the interactions between neutrons and atoms (displacement cascades) and to end up with the assessment of the ensuing evolution of steel mechanical properties. It therefore has to rely on a multi-scale approach ranging from the atomic level (nanometer and picosecond scales) up to the grain level (micrometer and year scales) and finally to the macroscopic level (centimeter and year scales), while retaining all the relevant information when linking successive levels. Such a complex simulation can only be done by modeling the involved physical phenomena. This section gives the hypothesis used in RPV-1 to model the formation of irradiation-induced damage and the plasticity behavior in RPV steels.

3.1. Modeling of the irradiation-induced damage

The hypotheses used to model the formation of the irradiation-induced damage are given hereafter. Some of them are in full conformity with the current state of knowledge described in the previous section: they are preceded by a (•). The other ones have been made to ease the building of RPV-1. They rely on the current knowledge but will have to be reconsidered for the subsequent versions of this VTR: they are preceded by a (♣).

- ♣ The irradiation-induced increase of yield stress is independent of the steel type (forging, plate, weld) and slightly depends on its metallurgical structure. Only the grain or lath size and the dislocation density have an influence (effects of size and distribution of carbides, shape of grains... are not accounted for).
- ♣ In its current version, RPV-1 does not take the intergranular segregation of phosphorus into account. Consequently, it cannot be used to forecast the behavior of steels containing more than about 150 ppm of phosphorus.

♣ The only chemical elements controlling the irradiation-induced hardening are Cu, Mn and Ni (Si is not allowed for, while carbon and nitrogen are indirectly taken into account by reducing the mobility of vacancies).

♣ The irradiation induces the formation of the four following types of hardening defects:
- ✓ 2-D SIA dislocation loops with {1 1 1} habit planes;
- ✓ spherical vacancy clusters;
- ✓ spherical copper-rich precipitates containing Mn and Ni atoms;
- ✓ spherical vacancy-solute (Cu, Mn, Ni) clusters.

• Primary knocked-on atoms (PKAs) induced by neutrons produce displacement cascades which may split into sub-cascades. They also produce some point defects between the sub-cascades.

• Alloying elements and impurities do not affect:
- ✓ the generation of PKAs and (sub)-cascades[1];
- ✓ the 'collision' and 'recombination' phases of (sub)-cascades;
- ✓ the production and distribution of point defects between the sub-cascades.

These phenomena are also supposed to be temperature-independent between 0 and 600 K. Consequently, they can be simulated in pure iron at any temperature below 600 K.

• During their 'collision' and 'recombination' phases, (sub)-cascades belonging to the same cascade or to different cascades do not interact; they neither interact with any defect migrating in the bulk. They can therefore be simulated separately.

♣ At the end of their recombination phase (some tens of picoseconds), each (sub)-cascade leaves isolated or clustered surviving point defects. The short-term evolution (some milliseconds) of these defects occurs without any interaction with other (sub)-cascades or migrating defects, and can thus be simulated separately.

♣ Cu is the only alloying element playing a role in the short-term evolution (some milliseconds) of the point defects left by the (sub)-cascades. This evolution can therefore be simulated in a Fe–Cu alloy and can be described as follows:
- ✓ SIAs and SIA clusters migrate (1D/3D migration) from the (sub)-cascade area to the bulk, some of them may have merged or interacted with surviving vacancies (leading to the annihilation of SIAs and vacancies). In the bulk, they may act as nuclei of SIA dislocation loops or interact with pre-existing hardening defects or other features (grain boundaries, dislocations,...).
- ✓ vacancies and vacancy clusters have a 3-D migration in the (sub)-cascade area. Their number density in this area is high enough for some of them to merge and/or to collect some copper atoms, which leads to the formation of nuclei of hardening defects in the (sub)-cascade area: small vacancy clusters, vacancy-copper atom clusters or pure copper clusters.

In the following part of the document, the defects (SIAs, SIA clusters, vacancies, vacancy-copper clusters,...) resulting from the short term evolution of the surviving point defects left by a (sub)-cascade will be called 'nuclei of hardening defects' produced by the (sub)-cascade.

• When a displacement (sub)-cascade is generated within a sphere of radius R_{int} centered on a pre-existing hardening defect, its residual point defects are supposed to be attracted by this defect and to annihilate each other on it. Thus, the cascade has no effect. The probability of occurrence of such an event is given by [6]:

$$P(t) = 1 - \exp(-GV_{int}t), \quad (1)$$

where G is the (sub)-cascade generation rate ($cm^{-3}s^{-1}$); V_{int} is the interaction volume, $V_{int} = 4\pi R_{int}^3/3$; $R_{int} = 1$ nm in the current version of RPV-1; t is the irradiation time.

♣ The surviving vacancies created between the sub-cascades are isolated while the SIAs are distributed as follows: 60% are isolated, 20% are in clusters of size 2, 10% in clusters of size 3, 6% in clusters of size 4, 3% in clusters of size 5 and 11% in clusters if size 6. It is supposed that all these point defects do not have a high enough number density in their production area to significantly interact with each other or with solute atoms and to form nuclei of defects. Most of them therefore migrate into the bulk.

• If the copper content in the solid solution is high enough (>0.1%), nuclei of pure copper precipitate may also appear in the bulk through a classical thermal germination process accelerated by the irradiation.

♣ Copper enrichment of hardening defects occurs by enhanced and induced precipitation (cf. Section 2.2.1). It means that copper atoms reach these defects by the two following mechanisms:
- ✓ a random walk mechanism which is accelerated by the super-saturation of vacancies.
- ✓ a migration induced by an interaction with fluxes of vacancies (interaction with SIAs is not accounted for in the current version of RPV-1, since first principle calculations showed that the interaction between copper and SIA is negligible [54]).

[1] The term (sub)-cascade covers a sub-cascade or a displacement cascade which cannot split into sub-cascades (PKA recoil energy <40–50 keV).

♣ As hardening defects are enriched in copper, they get also enriched in Ni, Mn. This enrichment relies on an irradiation enhanced diffusion mechanism and takes into account the interface between the matrix and the defects. In RPV-1, the numbers of Mn and Ni atoms in each defect are considered to be proportional to the number of copper atoms in the defect. The proportionality factors are estimated at the thermodynamic equilibrium (equality of the chemical potentials in the matrix and in precipitates). It is also supposed that the thermodynamic principles are not applicable for defects containing less than five copper atoms. Consequently, only defects containing more than five copper atoms are enriched in Mn and Ni atoms.

- Hardening defects may emit solute atoms, vacancies or SIAs through thermal-activated processes. Differences between emission and absorption rates lead to the dissolution of defects and the growth of others.

3.2. Modeling of the plasticity behavior

Irradiation-induced defects constitute obstacles to the gliding of dislocations and thus have a hardening effect. In RPV-1, the assessment of this hardening is made with a Foreman and Makin-type code [71], named DUPAIR. Such a code is aimed at assessing the increase of the resolved shear stress of a monocrystal due to the presence of obstacles with different strength levels. It relies on several hypotheses and simplifications which are well described in the open literature (e.g. [71]). The most important ones are the following:

- The grain is described by its shear modulus and Poisson ratio.
- The dislocation is described by its tension line and Burgers vector.
- The obstacles are supposed to be punctual (pinning points) and are described by the pinning force they exert on the dislocation line.
- Only one dislocation move in the material. It cannot leave its slip plane (no cross-slip or climbing).
- When an external stress is applied, each segment of dislocation line between two obstacles bows and takes the shape of an arc of circle (i.e. the tension line remains constant along the segment whatever its curvature). This is a strong approximation, particularly when the Peierls friction stress is high: e.g. screw dislocation in Fe below room temperature.
- The dislocation can pass any obstacle when:
  - ✓ the resultant of the tension lines on each side of the pinning point is higher than the pinning force;
  - ✓ the two segments of dislocation line on each side of the obstacle are parallel (Orowan process).

RPV-1 also relies on the hypothesis that:

- The plasticity of irradiated RPV steels is controlled by the gliding of screw dislocations (this hypothesis is verified for non-irradiated RPV-steel at a temperature up to 20 °C but has never been verified after irradiation).
- The lattice friction (Peierls stress) exerted on screw dislocations is supposed to be independent of the presence of the irradiation-induced defects.
- Above room temperature, the dislocations can pass the smallest defects (some atoms or point defects) by thermally activated mechanisms; hence, these defects have no hardening effect [72]. The procedure used to determine the pinning forces exerted by the irradiation-induced defects on a screw dislocation is presented in Section 4.3.2.
- In copper-rich precipitates and vacancy-solute (Cu, Mn, Ni) clusters, Ni and Mn atoms are supposed to have the same 'hardening effect' as copper atoms. Thus, for the hardening assessment, these defects are considered to contain only one type of solute atoms: copper atoms.

4. Description of RPV-1

As already mentioned, RPV-1 is an integrated computer tool aimed at simulating irradiation effects in pressure vessel steels of LWRs. It was built with the objective that its input and output data would be similar to those of experimental irradiation programs carried out for assessing the in-service behavior of such steels (Fig. 2). Its inputs are the irradiation conditions (neutron spectrum, temperature and time of irradiation), characteristics of the non-irradiated steel (Cu, Mn, Ni contents, grain size,...) and the conditions of a tensile test (temperature and deformation rate). The description of the irradiation-induced evolution of the microstructure and the concomitant increase of the yield stress are its output data. By using theoretical or empirical correlations, the irradiation-induced shift of the Charpy brittle ductile transition temperature can be determined from the increase of the yield stress (e.g. [13]). Section 4.1 provides a description of the overall architecture of RPV-1 i.e. the way the used codes have been linked up together and connected to the databases. In Section 4.2, a brief description of these codes and the procedures followed to build up the databases are given. Finally, the successive steps of a simulation are explained.

4.1. Architecture of RPV-1

RPV-1 is made of five codes and two databases. Its architecture is sketched in Fig. 3, and may be described

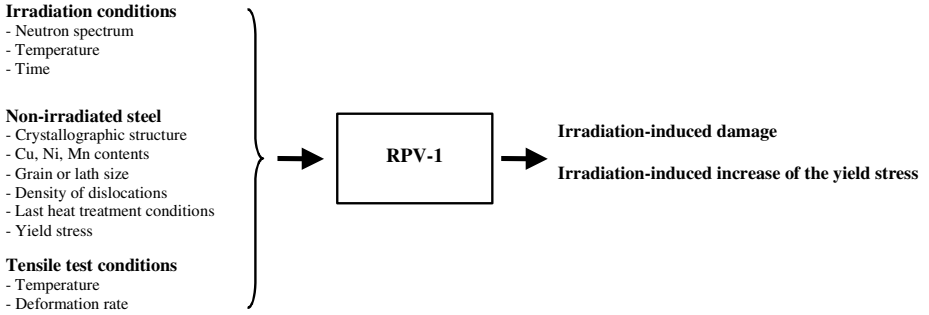

Fig. 2. Input and output data of RPV-1.

as a stack of 'racks'. Each of these racks contain a code or a database and are linked up so as to receive, treat and/or transmit data. Built in that way, RPV-1 is an evolutionary tool and can be improved very easily: as soon as a new code or model is available, it can be implemented without any difficulty by replacing a 'rack' by a new one. The codes and databases used in RPV-1 are accompanied by pre- and post-treatment scripts in order to link them together and transmit data. They are also embedded in a Python interface which eases the running of the simulations and the visualization of the results. The main board of this interface (Fig. 4) is used to select inputs concerning the irradiation conditions (neutron spectrum, irradiation time and temperature), steel (%Cu, %Ni, %Mn) and tensile test (temperature, deformation rate). Auxiliary boards are also available to select complementary steel input data (grain size, dislocation density) and all the physical parameters required by the codes (point defect formation energies, defect migration energies...).

As seen in Fig. 3, three modules can be identified in RPV-1, they can be run separately:

- the '*short-term irradiation*' module treats the neutron spectrum to provide the PKA spectrum (with the code SPECMIN, see Section 4.2.1) and then, the (sub)-cascade spectrum in pure iron (with the code INCAS, Section 4.2.2). By convoluting the (sub)-cascade spectrum (number of (sub)-cascades versus their dissipated energy) and the size distribution of nuclei of hardening defects produced by each (sub)-cascade (given in the database CASCADE, see Section 4.3.1), it defines a part of the source term for the long-term irradiation module. The generation rate of point defect (isolated or clustered) between the sub-cascades is the other part of this source term.
- the '*long-term irradiation*' module mainly includes a Rate Theory code (so-called MF-VISC, see Section 4.2.3) to simulate the evolution of the irradiated microstructure from about 10^{-3} s to years. This module continuously checks the evolution of the microstructure so as to adjust the source term to account for: (i) the evolution of the free copper content in the matrix; (ii) the interaction of displacement cascades with pre-existing defects.

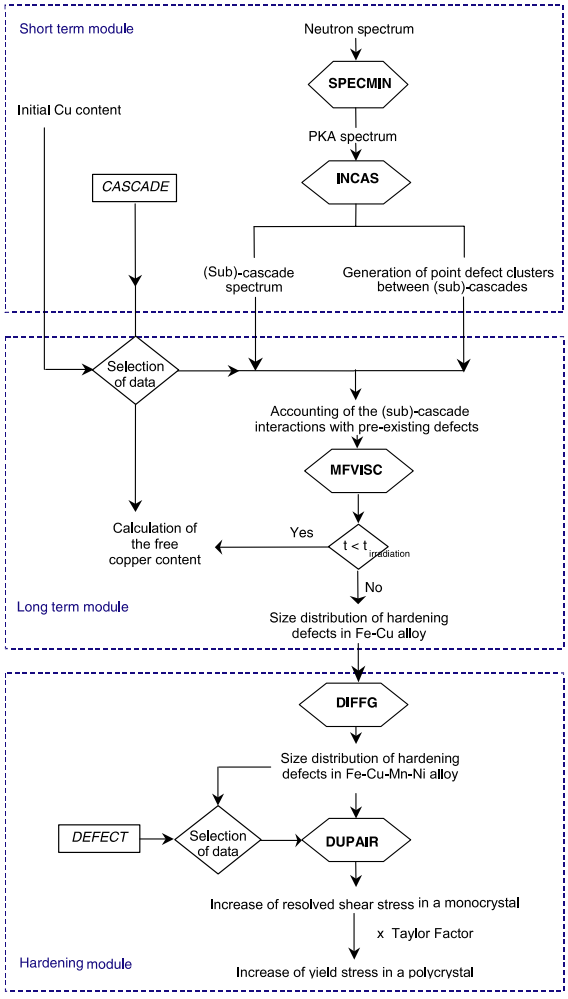

Fig. 3. Schematic structure of RPV-1. To simplify the figure, only two input data (neutron spectrum and initial copper content) are indicated.

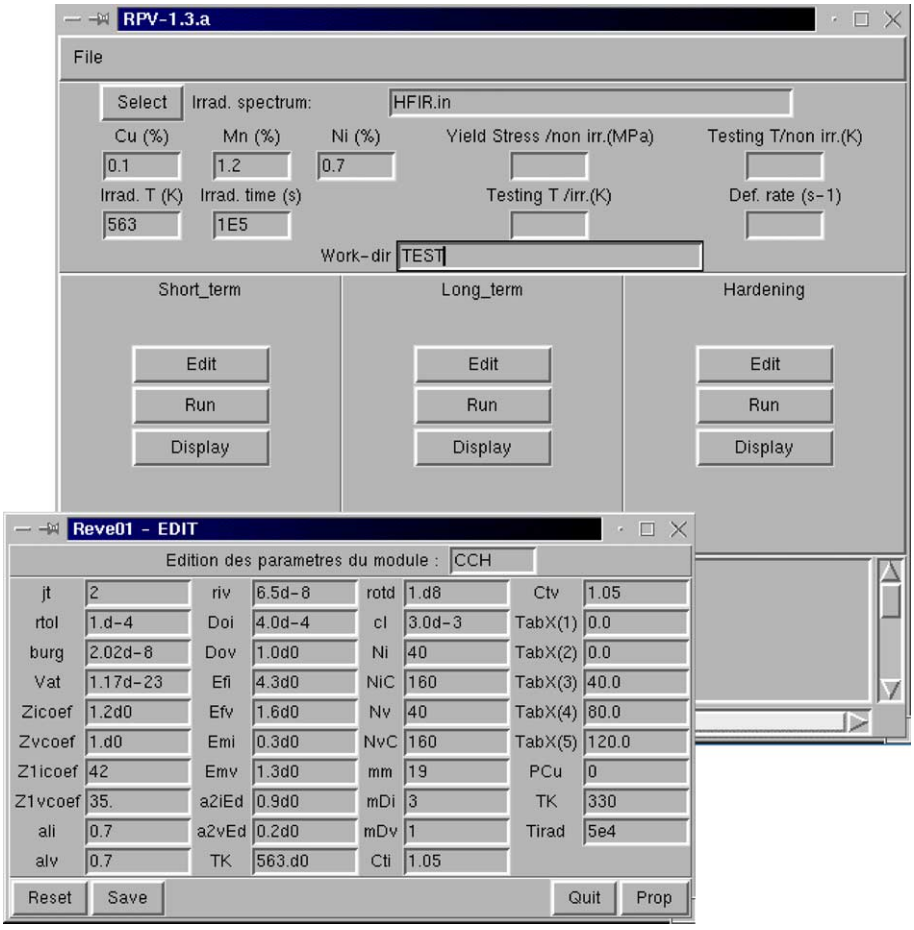

Fig. 4. Python user's friendly interface of RPV-1. Main board used to select input data concerning the irradiation conditions, steel and tensile test; one of the auxiliary boards to select complementary steel input data and physical parameters.

- the '*hardening*' module finalizes the simulation of the formation of the hardening defects by enriching those containing Cu with Ni and Mn, using results provided a kinetic-thermodynamic code (so-called DIFFG, see Section 4.2.4). It also simulates a tensile test with a mesoscopic code (the Foreman and Makin code called DUPAIR, see Section 4.2.5), using a database of pinning forces (called DEFECT).

4.2. Codes used to build RPV-1

This section provides a short description of the codes used to build-up RPV-1. Among them, SPECMIN, INCAS, MFVISC, DIFGG and DUPAIR are directly chained in RPV-1 (see Fig. 3). Two codes, DYMOKA and LAKIMOCA, were used to build up the two databases CASCADE and DEFECT integrated in RPV-1.

4.2.1. SPECMIN

SPECMIN is a simplified version of the code SPECTER; both codes have been developed by L. Greenwood from Pacific Northwest National Laboratory [73]. SPECMIN provides less information than SPECTER, but allows the simulations to be operated on a PC-type computer with typical running times of a few seconds. It is written in FORTRAN.

SPECMIN relies on the binary collision approximation (BCA) and simulates the interactions between neutrons and atoms of pure elements. It takes the elastic collisions into account as well as inelastic interactions and all possible direct nuclear reactions, such as (n,p), (n,α), $(n,2n)$ etc., between both kinds of particles. All these phenomena are characterized by differential neutron cross-sections available from the evaluated nuclear data file database (ENDF). ENDF data and their uncertainties can be obtained from the National Neutron

Cross-Section Center at Brookhaven National Laboratory (USA). For a given neutron spectrum, the calculations with SPECMIN successively lead to the following results:

- the PKA spectrum (number of PKAs expressed as a function of PKA's recoil energy) in which the PKAs are classified and counted with respect to energy groups. For the subsequent calculations, all the PKAs belonging to the same group are considered as dissipating the same energy, i.e. the middle group energy. The gas production is also calculated from the nuclear reactions;
- the 'damage energy'[2] (T_{dam}) of PKA's calculated from their recoil energy according to the Lindhard's theory [74];
- the dpa rate calculated from the Norgett, Robinson and Torrens expression (NRT dpa [75]) giving the total number (N_s) of atoms displaced per PKA: $N_s = 0.8T_{dam}/2E_d$ (E_d is the minimal energy required to displace an atom from its lattice site).

4.2.2. INCAS

INCAS has been developed by S. Jumel and J.C. Van Duysen from Electricité de France [10] and is written in FORTRAN. It is based on the binary collision approximation and simulates the fate of PKAs from the time they are knocked by a neutron, up to the time they spread all their kinetic energy and thus stop their moving. It forecasts their elastic collisions with lattice atoms and interactions with electrons. INCAS provides the average number and the size of the damage zones (zone where Frenkel pairs are produced) induced by the PKAs according to their recoil energy. It also provides the distance between successive damage zones and the energy dissipated[3] in each of them. Two cases have been identified:

- damage zones in which the dissipated energy is higher than 8.3 keV are considered as (sub)-cascades. They are classified and counted with respect to five dissipated energy groups: 5–15, 15–25, 25–35, 35–45, 45–55 keV (the (sub)-cascade spectrum). For the subsequent calculations, all the (sub)-cascades belonging to a same group are considered as dissipating the same energy, i. e. the middle group energy;
- damage zones in which the dissipated energy is lower than 8.3 keV are considered to produce Frenkel pairs between the (sub)-cascades. At the end of the recombination phase, the number of surviving Frenkel pairs left by each of these damage zones can be estimated with the expression (defined by Molecular Dynamics simulations [41]):

$$v(E) = 5(T_{dam})^{0.74}, \quad (2)$$

where T_{dam} is the damage energy, in keV. The surviving SIAs and vacancies may be isolated or clustered in small nuclei (SIAs: 60% are isolated, 20% in clusters of size 2, etc.; see Section 3.1).

Among the data provided by INCAS, those directly used in RPV-1 are the (sub)-cascade spectrum and the Frenkel pairs generation rate between the (sub)-cascades.

4.2.3. MF-VISC

MF-VISC (mean field vacancy interstitial solute clusters) is a Rate Theory code developed by A. Barbu (CEA), V. Duwig (EDF) and S. Jumel (EDF) from the MF-VIC code [76,77]; it is written in FORTRAN. For the building of RPV-1, MF-VISC was used to reproduce the long-term evolution of the irradiation-induced damage. In its current version, it simulates the fate of the vacancies, copper atoms and SIAs clusters. The vacancy clusters and SIA dislocation loops containing up to 20 elements can be mobile, their mobility are parameters of the code. The other defects are immobile. A detailed presentation of MF-VISC is available in [78].

4.2.4. DIFFG

In RPV-1, Mn and Ni atoms are introduced into the simulation with the DIFFG code, developed by B. Odette from the University of California in Santa Barbara and B. Wirth from the University of California in Berkeley [37,79]. DIFFG is a kinetic-thermodynamic code written in FORTRAN, which determines the phase stability in a Fe–Cu–Mn–Ni system by taking into account the influence of the precipitate–matrix interfaces. The precipitate evolution is modeled by tracking the flows of alloying atoms imposed by the difference of chemical potentials between the matrix and the precipitates and accelerated by the vacancy super-saturation induced by irradiation. The cluster radius and composition are followed as a function of time until each alloying atoms has the same chemical potential in the matrix and the precipitates. The final ratios of the Mn and Ni contents over the Cu content in the precipitates are then calculated. They are used to determine the Mn and Ni enrichments of the Cu-bearing hardening defects simulated with the MF-VISC code.

4.2.5. DUPAIR

DUPAIR is used to assess the irradiation-induced hardening. It is a Foreman- and Makin-type code developed at EDF by S. Jumel, C. Domain and J.C. Van Duy-

[2] Damage energy = energy spread in atomic collisions.

[3] Dissipated energy = energy spread in atomic collisions and electronic interactions.

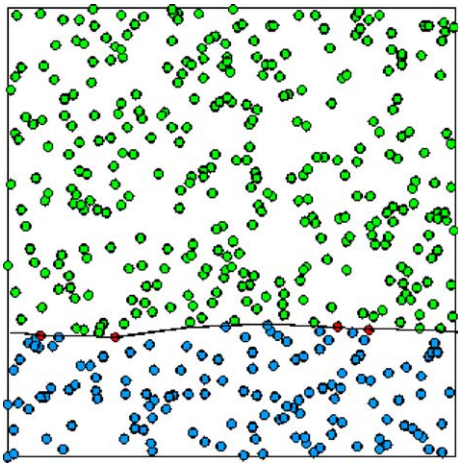

Fig. 5. Simulation with the DUPAIR code: bowing of a dislocation line pinned on irradiation-induced defects.

sen from EDF [80]; it is written in C language. In DUPAIR, the studied material is represented as a parallelepipedic box and the different types of irradiation-induced defects are randomly distributed according to their number density, each defect being characterized by its type, size and pinning force. The code simulates the gliding of one dislocation line in the mid-plane of the box (Fig. 5). The maximal shear stress required to make the dislocation cross this box is considered as the irradiation-induced increase of the resolved shear stress of a monocrystal. It is multiplied by the Taylor factor (≈3) to get the increase of yield stress of the poly-crystalline material, which is assimilated to the increase of the conventional yield stress $\Delta R_{P0.2}$. As already mentioned, the irradiation-induced shift of the Charpy brittle ductile transition temperature can be determined from this increase of the yield stress by using empirical and theoretical correlations.

4.2.6. DYMOKA

DYMOKA is a Molecular Dynamic code developed by C. Domain from EDF (e.g. [81]); it is written in C language. For the building of RPV-1, its parallel version was used to simulate displacement (sub)-cascades in iron as well as the interactions between hardening defects and a screw dislocation. The used EAM-type inter-atomic potentials are given in Table 1.

4.2.7. LAKIMOCA

LAKIMOCA is a so-called Kinetic Monte Carlo code developed by C. Domain from Electricité de France (e.g. [40]); it is written in C language. For the building of RPV-1, LAKIMOCA was used to simulate the formation of nuclei of hardening defects during the short term evolution (some milliseconds) of the residual point defects left by displacement (sub)-cascades. It takes a large number of types of object (solute atoms, impurities, point defects clusters, vacancy-solute clusters, grain boundaries,...) into account and can be used with two models: Atomistic Kinetic Monte Carlo or Object Kinetic Monte Carlo according to the nature of the object considered as mobile. With the former, the interactions between atoms are described with EAM inter-atomic potentials (Table 1); with the latter, these interactions are not explicitly described.

Table 1
References of EAM-interatomic potentials used to carry out the simulations with DYMOKA and LAKIMOCA

		Ref.
Fe–Fe	Ludwig et al.	[88]
	Raulot	[89]
Cu–Cu	Ludwig et al.	[88]
Fe–Cu	Ludwig et al.	[88]

- *The Atomic Kinetic Monte Carlo model* considers the mobility of vacancies only. At each time step, one vacancy jumps to one of its nearest sites or is emitted from an object (vacancy clusters,...). The physical inputs of the model are the jump frequencies of vacancies depending on their local environment and the vacancy emission frequencies of the objects depending on their type and size. With this model, the current version of LAKIMOCA cannot simulate the fate of SIAs.
- *The Object Kinetic Monte Carlo* model takes the mobility of several types of objects into account: isolated point defects, point defect clusters, vacancies-solute clusters, solute precipitates,... At each time step, one of these objects either moves of one inter-atomic distance or emits one element (point defect or solute atom). The physical inputs of the model are the jump and emission frequencies of the objects. Several parameters describing the simulated material like the migration energies of point defects, the binding energies of point defects with point defect clusters, the binding energy of Cu atoms with vacancies... are also required.

Both models take into account the presence of sinks (dislocations, grain boundaries,...) where point defects may disappear.

4.3. Databases used in RPV-1

Some calculations required to simulate irradiation effects are extremely computer-time consuming. They cannot be performed in flexible versions of VTRs usable on PCs. For RPV-1, these calculations were carried out separately on powerful parallel computers (CRAY, PC clusters,...) and their results were stored in databases

integrated in the reactor. During the simulation, the needed data are taken from these databases.

As already mentioned, two databases have been integrated in RPV-1:

- the 'CASCADE' database which contains the size distributions of nuclei of hardening defects formed by the surviving point defects left by (sub)-cascades in Fe–Cu alloys. These data are used to prepare the source term of the Rate Theory code MF-VISC.
- the 'FORCE' database which contains the values of the pinning force exerted by the irradiation-induced defects on a screw dislocation. These data are used as input data of the DUPAIR code to calculate the irradiation-induced hardening.

The CASCADE and FORCE databases were built as described in the two following sections.

4.3.1. CASCADE

The size distribution of nuclei of hardening defects formed within some milliseconds (short term evolution) by the surviving point defects left by (sub)-cascades in Fe–Cu alloy are stored in CASCADE, depending on the:

- irradiation temperature (T),
- damage energy in the (sub)-cascade (T_{dam}),
- free copper content in the matrix (Cu).

The current version of CASCADE includes results for $T = 333$, 423 and 573 K; $T_{dam} = 10$, 20, 30 and 40 keV; Cu = 0.00, 0.03, 0.10, 0.20 and 0.30 at.% Cu. The main steps of its building are described hereafter and summarized in a more intelligible way in Fig. 6:

- displacement (sub)-cascades with PKA damage energy of 10, 20, 30 or 40 keV were simulated by Molecular Dynamics in pure iron at $T = 600$ K (the results are supposed to be temperature independent in the range 100–600 K). The simulations were stopped when the configuration of the surviving defects did not significantly evolve anymore (about 10 ps of physical time). For each PKA energy, three simulations were performed with different initial moving directions of the PKA.
- the short term evolution (some milliseconds) of the surviving point defects left by the (sub)-cascades was simulated with LAKIMOCA in Fe–Cu alloys: copper was introduced in the simulation by replacing iron atoms by copper atoms in the simulation box containing the surviving defects. For each PKA initial condition (energy and direction), simulations were carried out at three temperatures ($T = 333$, 423 or 573 K) and with four copper contents (Cu = 0.00, 0.03, 0.10, 0,20 or 0.30 at.%). For each set of copper content, temperature and PKA initial energy, the simulation sequence was:
  - ✓ Firstly the Object Kinetic Monte Carlo (OKMC) was applied to follow the fate (diffusion, clustering,...) of the SIAs during a few microseconds. The simulation was stopped when the configuration of SIAs did not significantly evolve anymore

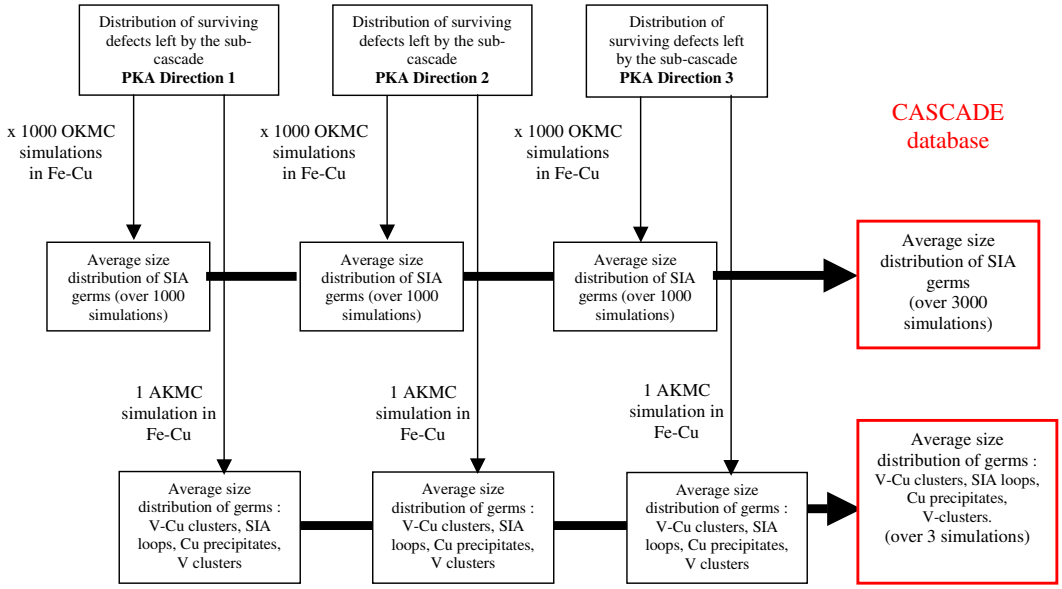

Fig. 6. Building of the CASCADE database. Simulations carried out for a given set of irradiation temperature, PKA energy and copper content.

(most of them have left the simulation box; some may have merged to form clusters or may have been annihilated with surviving vacancies). The mobility of SIAs is much higher than that of vacancies, hence the vacancies remained almost immobile during the simulation. This OKMC simulation was carried out 1000 times with different initial random selection numbers.

The final size distribution of nuclei of SIA loops was determined by averaging the size distributions provided by the 3000 simulations (simulations for 3 PKA initial directions × 1000 OKMC simulations).

✓ Then, the Atomic Kinetic Monte Carlo was used to follow the fate of the surviving vacancies during about some milliseconds. The simulation was stopped when the configuration of the vacancies and copper atoms did not significantly evolve anymore. For each set of conditions, this simulation was carried out only once due to its high computing requirement. The final size distribution of nuclei of vacancy-copper cluster, vacancy cluster and copper precipitate was determined by averaging the size distributions provided by the three simulations corresponding to the different PKA initial directions.

Finally, the size distribution of nuclei of hardening defects has been stored in CASCADE according to the irradiation temperature, PKA energy and copper content.

4.3.2. FORCE

As already mentioned, FORCE contains the pinning forces exerted by the hardening defects (vacancy clusters, SIA dislocation loops, pure copper precipitates and vacancy-copper clusters) on a screw dislocation. These forces have been determined by Molecular Dynamics simulations using a 'static approach'. This means that the dislocation remains fixed in the simulation box (only displacements of atoms related to the box relaxation are allowed) and different positions of the defects as regards to the dislocation are considered. This approach is precisely described in [11], it can be summarized in the following way (Fig. 7) [24,82]:

- the screw dislocation is introduced at the center of the simulation box by applying its displacement field to the atoms, as described in [83];
- the studied hardening defect is successively introduced at different distances from the dislocation core;

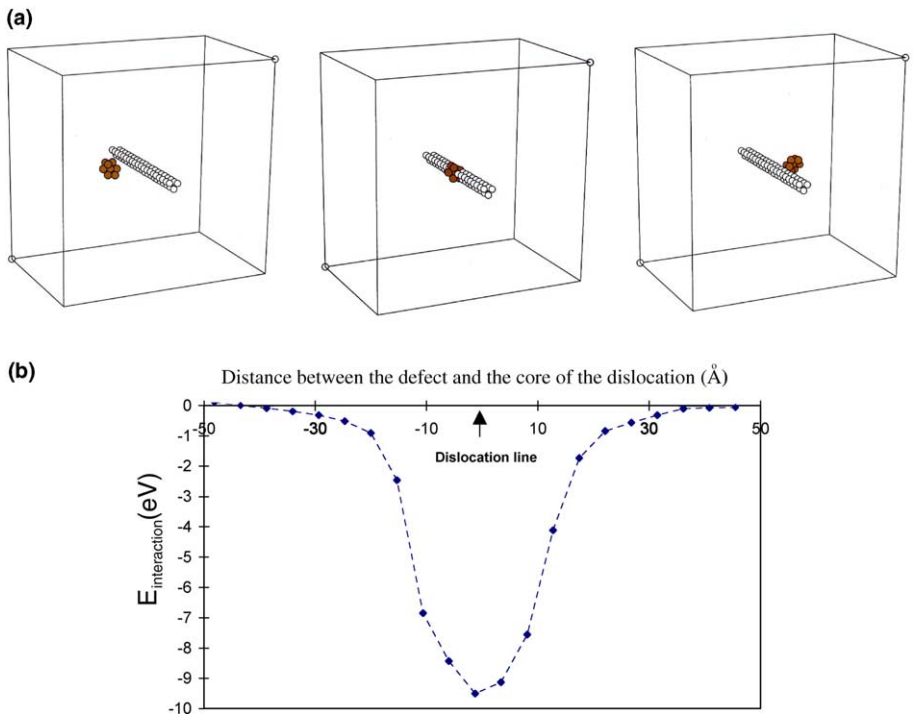

Fig. 7. Static approach used to study the interaction between a screw dislocation and hardening defects with the Molecular Dynamics code DYMOKA [6]. (a) Three configurations of a 9 copper atoms precipitate and the screw dislocation; (b) Variation of the interaction energy between a 600 copper atoms precipitate and the screw dislocation, as a function of their separation distance.

- for each configuration, the relaxed energy of the system is calculated. The interaction energy between the two features is defined as the relaxed energy for the considered configuration minus the relaxed energy when they are largely separated (thus do not interact);
- the pinning force of the defect is defined as the maximum slope of the curve giving the interaction energy of the system versus the distance between the defect and the dislocation.

As an example, Fig. 7(b) shows results obtained from a pure copper precipitate. Such simulations have been carried out for each type of defects (vacancy clusters, SIA dislocation loops, pure copper precipitates and vacancy-copper clusters) with different size and content. The results are stored in the FORCE database as obtained or in an analytical form according to the nature of the hardening defect. Detailed results are published elsewhere [11].

The used 'static' approach is very simplified and deserves to be replaced by a dynamic one in which the dislocation would be mobile and the defect fixed. However, the simulation of the gliding of a screw dislocation in bcc iron-base alloys is not an easy task. Indeed, due to the Peierls friction force, this gliding requires the generating and propagating of kinks along the dislocation line.

4.4. Simulation steps of RPV-1

The simulation of irradiation effects with RPV-1 requires the successive activating of the three modules presented in Section 4.1. The successive steps are described hereafter and illustrated in Fig. 8 for a simulation carried out at 150 °C with a neutron spectrum which is representative of one of the irradiation channels of the French reactor OSIRIS (composition of the irradiated steel: 0.1%Cu, 1.3%Mn, 0.7%Ni; flux $\approx 4.4 \times 10^{16}$ n.m^{-2} s^{-1}, $E \geqslant 1$ MeV).

For the 'short term irradiation' module:

Step 1:
The PKA spectrum and the dpa rate are determined from the neutron spectrum with the SPECMIN code. As already mentioned, the effects of alloying elements and impurities on both quantities are negligible and consequently the simulation is carried out in pure iron (Fig. 8(a) and (b)).

Step 2:
The (sub)-cascade spectrum is determined from the PKA spectrum with the INCAS code. The effects of alloying elements and impurities on (sub)-cascade formation are also negligible and the simulation is consequently carried out in pure iron (Fig. 8(c)). The INCAS simulation provides also the number of Frenkel pairs produced between the (sub)-cascades by time and volume units. As already mentioned, it is supposed that the corresponding vacancies are isolated and the SIAs distributed to the following nuclei: 60% are isolated, 20% are in clusters of size 2, 10% in clusters of size 3, 6% in clusters of size 4, 3% in clusters of size 5 and 11% in clusters if size 6.

Step 3:
The size distributions of nuclei of SIA loops, copper precipitates, vacancy clusters and vacancy-copper atom clusters created by the (sub)-cascades are read in the CASCADE database as function of the damage energy in the (sub)-cascade, the irradiation temperature and the content of free copper in the solid solution. They are introduced as source terms in the rate theory code MF-VISC according to the (sub)-cascade spectrum. To be more precise, let us consider the following example:

- ✓ The (sub)-cascade spectrum indicates that the irradiation introduces z cascades with a dissipated energy of 20 keV (corresponding to a damage energy of 15 keV) per time and volume units.
- ✓ CASCADE indicates that a 15 keV damage energy cascade creates an average of x_i SIA nuclei of size i and y_{jk} copper-vacancy nuclei containing j vacancies and k copper atoms, ...
- ✓ Then, $z \cdot x_i$ SIA nuclei of size i, $z \cdot y_{jk}$ copper-vacancy nuclei containing j vacancies and k copper atoms, ... are introduced as source term in MF-VISC per time and volume units. This operation is done for each group of (sub)-cascade damage energies.

If the free copper content of the steel is not one of those taken into account in CASCADE, the corres- ponding size distribution of nuclei is determined by interpolating between the two distributions related to the closest copper contents already existing in CASCADE. As an example: if for a 20 keV (sub)-cascade CASCADE indicates n_i and m_i nuclei of three SIAs when the copper contents are 0.03% and 0.1% respectively; then, for any copper content X such as $0.03\% < X < 0.1\%$, the source term taken into account for nuclei of three SIAs is equal to:

$$\frac{1}{(0.1 - 0.03)}[m_i(X - 0.03) + n_i(0.1 - X)]. \quad (3)$$

The same interpolation is done for all the nuclei. The mono vacancies and SIA nuclei produced between the sub-cascades are also added into the source term of MF-VISC.

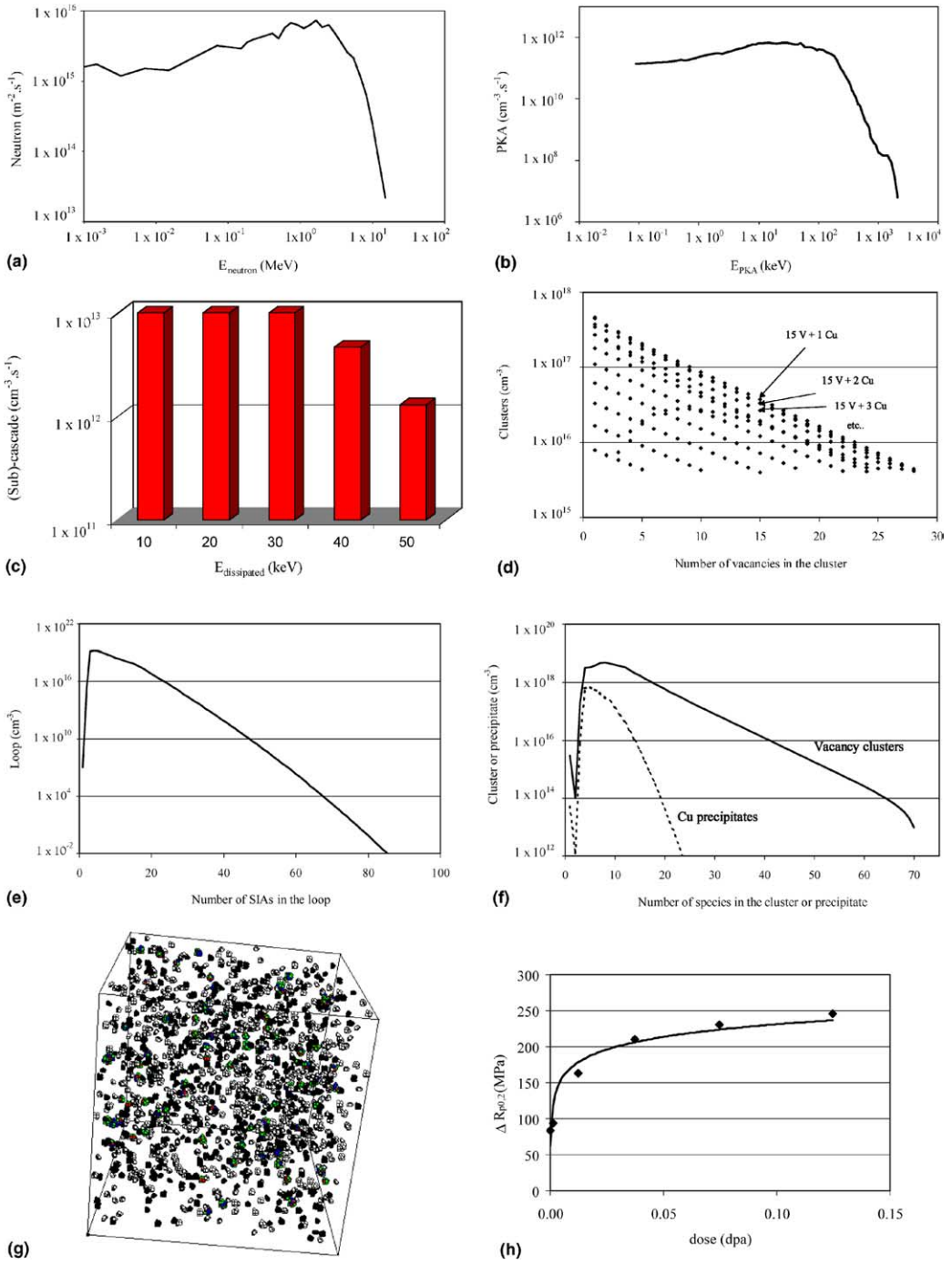

Fig. 8. Simulation of irradiation effects at 150 °C in a 0.1%Cu, 0.7%Ni, 1.3%Mn steel with a neutron spectrum representative of one irradiation channel of the French reactor OSIRIS (flux $\approx 4.4 \times 10^{16}$ n.m^{-2}s^{-1}, $E \geqslant 1$ MeV). (a) Neutron spectrum; (b) PKA spectrum in pure iron; (c) (sub)-cascade spectrum in pure iron; (d) size distribution of vacancy-copper clusters for a dose of 0.1 dpa. (e) Size distribution of SIA loops for a dose of 0.1 dpa; (f) size distribution of vacancy clusters and copper precipitates for a dose of 0.1 dpa; (g) distribution of hardening defects for a dose of 0.1 dpa; (h) evolution of the yield stress versus the dose. (Vacancy: white, SIA: black; Cu: red, Mn: green, Ni: blue; box size: $28.7 \times 28.7 \times 28.7$ nm^3.)

For the 'long term irradiation' module:

Step 4:

The simulation with MF-VISC is carried out until the required irradiation time or number of dpa is reached. Results related to 20 intermediate times are also available.

Step 5:

At each MF-VISC step, the source term is adjusted in order to take into account the evolution of the microstructure:

- ✓ The residual free copper content in the matrix is re-calculated and the source term is modified accordingly.
- ✓ The probability for sub-cascades to occur at a distance of less than 1 nm of a pre-existing defect, and thus to have no effect, is calculated with the expression (1). To keep 'useful' (sub)-cascades only, the (sub)-cascades spectra is modified: in each group of energy of the (sub)-cascade spectrum, the number of (sub)-cascades is multiplied by $1 - P(t)$.

For the 'hardening' module:

Step 6:

At the end of the MF-VISC simulation and for the six last intermediate times, copper precipitates and vacancy-copper clusters are enriched in Mn and Ni atoms according to the results of DIFFG. The final size distribution of each type of irradiation-induced defects is then plotted on a graph. The examples given in Fig. 8(d)–(f) show that:

- ✓ the number densities of SIA dislocation loops and vacancy clusters are pretty high, which suggests that these defects play a significant role in the irradiation-induced hardening;
- ✓ the number densities of vacancy-copper clusters is in conformity with experimental results;
- ✓ pure copper precipitates have been formed but their number density is lower than that of vacancy-copper clusters.

The hardening defects can also be represented all together in a 3-D box by supposing them uniformly distributed in the material (Fig. 8(g)).

Step 7:

For the last six outputs of MF-VISC, Ni and Mn atoms in copper-rich precipitates and vacancy-solute clusters are replaced by Cu atoms (see Section 3.2) and the pinning forces exerted by all the irradiation-induced defects are determined from the FORCE database. The six outputs are used as inputs for DUPAIR, which simulates the corresponding irradiation-induced increase of the yield stress. This evolution of the increase of yield stress is plotted versus the irradiation time, total fluence, fluence higher than 1 MeV and number of dpa (Fig.

Table 2
Main homogenisations done during a simulation with RPV-1

SPECMIN	• Homogenization of the neutron's fates (elastic collisions with lattice atoms,...). All the neutrons having the same energy are considered to have the same fate: i.e. the average fate provided by the cross-sections for the considered energy
INCAS	• Homogenization of PKA's energies. The PKAs are classified according to groups of energy; all the PKAs belonging to a same group are considered to have the same energy: i.e. the middle-group energy. The width of the group is increasing with increasing energy • Homogenization of PKA's fates (sub-cascade productions,...). All the PKAs with the same initial energy are considered to have the same fate: i.e. the average fate given by the collision cross-sections for the considered energy • Homogenization of the energies dissipated in (sub)-cascades. The (sub)-cascades are classified according to groups of dissipated energy (15–25 keV, 25–35 keV,...); all the (sub)-cascades belonging to a same group are considered to spread the same energy: i.e. the middle-group energy (10 keV, 20 keV,...) • Homogenization of the size distribution of the surviving point defects left by the small damage zones produced between the (sub)-cascades: 60% of their SIAs are isolated, 20% are in clusters of size 2, 10% in clusters of size 3,...
CASCADE database	• Homogenization of the nuclei of hardening defects. All the (sub)-cascades with the same dissipated energy are considered to produce the same nuclei of hardening defects
MF-VISC	• Homogenization of the size distribution of hardening defects within a grain • Homogenization of the behavior of all the defects having the same size and content (SIAs, vacancies and/or Cu atoms)
FORCE database	• Homogenization of the pinning forces of all the hardening defects having the same size and content (SIAs, vacancies and/or Cu, Mn and Ni atoms)
DUPAIR	• Homogenization of the irradiation response of all the steel grains
Taylor factor	• Homogenization of the distribution of the spatial orientation of grains

8(h)). The concomitant evolution of the Charpy transition temperature can be determined from empirical correlations, e.g. $\Delta TT \approx 0.68\Delta R_{P0.2}$ (at 20 °C, without intergranular rupture) [84].

5. Quality of the simulations with RPV-1

5.1. Sensitivity to the input data

The development of VTRs can be impaired by an intrinsic weakness of the multi-scale approach required to build such tools. Indeed, this approach necessitates the homogenisation of results (behaviours, energies, size distributions,...) before each time or space scaling up. Every homogenisation induces a loss of information which may alter the sensitivity of the tool to its input data. The main homogenisations done during a simulation with RPV-1 are summarized in Table 2. Considerable efforts would be required to quantify their individual or collective 'buffer' effects on the RPV-1 sensitivity. However, it has been checked that the collective effect is low in a large range of irradiation conditions (flux, temperature,...). The next sections give some examples of results obtained with the version 1.2 g of RPV-1.

5.1.1. Sensitivity to the copper content

RPV-1 was run to simulate the irradiation-response of four steels containing 0.05%, 0.10%, 0.20% or 0.30%Cu (and 1.45%Mn, 0.2%Ni). The four simulations were performed at 250 °C with a neutron spectrum representative of one irradiation channel of the British experimental reactor HERALD (flux $\approx 5 \times 10^{16}$ n.m^{-2}s^{-1}, $E \geqslant 1$ MeV).

The simulated irradiation-induced increases of yield stress up to a dose of 0.1 dpa are plotted versus the dose in Fig. 9(a). It can be noticed that the hardening grows with the copper content, which shows that RPV-1 is sensitive to the copper content. Fig. 9(b) and (c) show the final size distributions of the hardening defects in the 0.05% and 0.30%Cu steels for the dose of 0.1 dpa. The number density of defects containing copper clearly increases with the steel copper content.

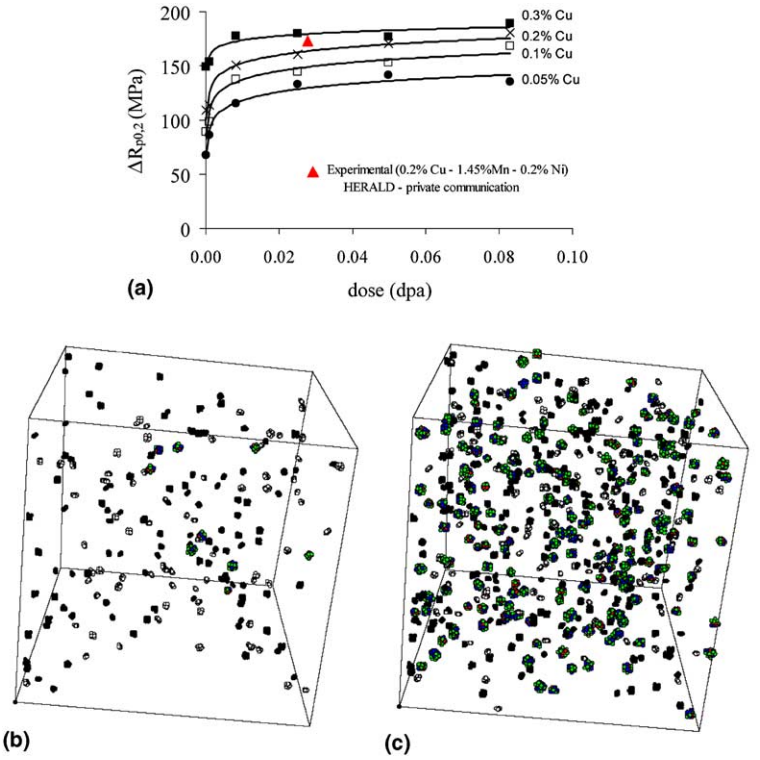

Fig. 9. Sensitivity of RPV-1 to the copper content. Simulation at 250 °C with a neutron spectrum representative of one irradiation channel of the British experimental reactor HERALD (steel with 1.45%Mn and 0.2%Ni; flux $\approx 5 \times 10^{16}$ nm^{-2}s^{-1}, $E \geqslant 1$ MeV). (a) Irradiation-induced increase of yield stress; (b) distribution of hardening defects for Cu = 0.05% and a dose of 0.1 dpa; (c) distribution of hardening defects for Cu = 0.3% and a dose of 0.1 dpa. (Vacancy: white, SIA: black; Cu: red, Mn: green, Ni: blue; box size: $28.7 \times 28.7 \times 28.7$ nm^3.)

5.1.2. Sensitivity to the irradiation temperature

RPV-1 was run to simulate the irradiation-response of a 0.05%Cu–1.3%Mn–0.7%Ni steel, at four temperatures ($T = 55$, 200, 250 and 300 °C). The simulations were performed with a neutron spectrum representative of one irradiation channel of the American experimental reactor HFIR up to a dose of 0.1 dpa (flux $\approx 2.6 \times 10^{19}$ n.m^{-2}s^{-1}, $E \geqslant 1$ MeV).

The simulated irradiation-induced increases of yield stress are plotted versus the dose in Fig. 10(a). It can be noticed that the hardening grows as the irradiation temperature decreases, which shows that RPV-1 is sensitive to the irradiation temperature. Fig. 10(b) and (c) show the final size distributions of the hardening defects for the irradiation carried out at 55 and 300 °C with a dose of 0.1 dpa. The number densities of SIA loops and vacancy clusters clearly increase as the irradiation temperature decreases.

5.1.3. Sensitivity to the neutron flux

RPV-1 was run to simulate the irradiation-response of a 0.05%Cu–1.3%Mn–0.7%Ni steel under four neutron fluxes. The simulations were carried at 55 °C with a dose up to 0.1 dpa. A neutron spectrum representative of one irradiation channel of HFIR was used as reference (flux $\approx 2.6 \times 10^{16}$ n.m^{-2}s^{-1}, $E \geqslant 1$ MeV). The other neutron spectra were obtained by multiplying this reference by 0.01, 0.1 or 10 (Fig. 11(a)). The procedure enables to study the flux effect without any changes in the spectrum shape.

The simulated irradiation-induced increases of yield stress are plotted versus the dose in Fig. 11(b). It can be noticed that the hardening grows as the neutron flux increases. However, the flux dependence tends to decrease with decreasing flux and becomes negligible between 0.1 HFIR and 0.01 HFIR. This trend is coherent with results obtained by Odette et al. in the same range of temperature [85]. These results show that RPV-1 is sensitive to the neutron flux. Fig. 11(d) and (e) provide the final size distributions of the hardening defects after irradiation with the highest and lowest neutron fluxes. The role played by the point defects clearly grows with increasing flux.

5.1.4. Sensitivity to the neutron spectrum

RPV-1 was run to simulate the irradiation response of a 0.1%Cu –1.3%Mn – 0.7%Ni alloy under two neutron spectra corresponding to the same dpa rate. The

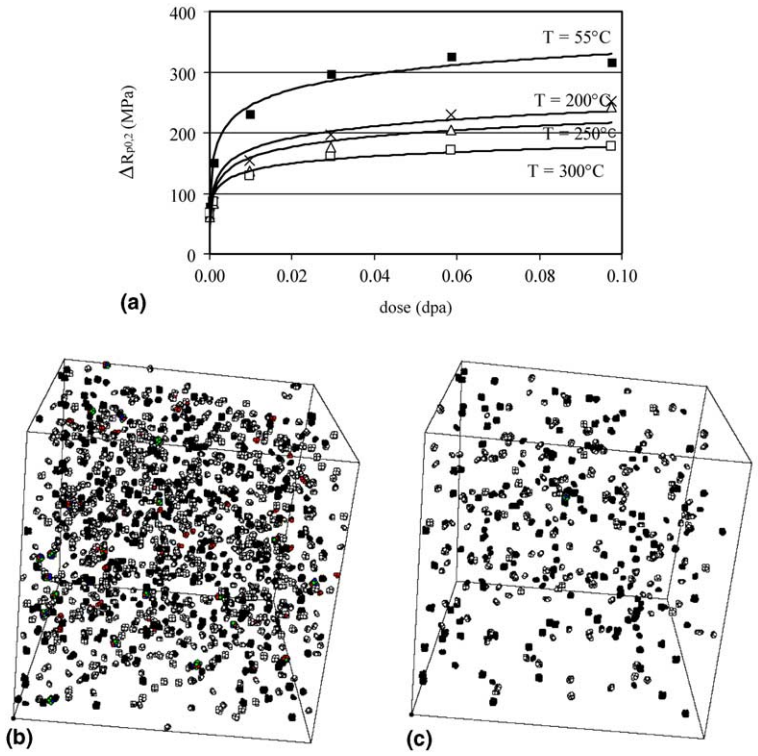

Fig. 10. Sensitivity of RPV-1 to the irradiation temperature. Simulations at 55, 200, 250 and 300 °C with a neutron spectrum representative of one irradiation channel of the American experimental reactor HFIR (steel: 0.05%Cu–1.3%Mn–0.7%Ni; flux $\approx 2.6 \times 10^{19}$ n.m^{-2}s^{-1}, $E \geqslant 1$ MeV). (a) Irradiation-induced increase of yield stress; (b) distribution of hardening defects for $T = 55$ °C and a dose of 0.1 dpa; (c) distribution of hardening defects for $T = 300$ °C and a dose of 0.1 dpa. (Vacancy: white, SIA: black; Cu: red, Mn: green, Ni: blue; box size: $28.7 \times 28.7 \times 28.7$ nm^3.)

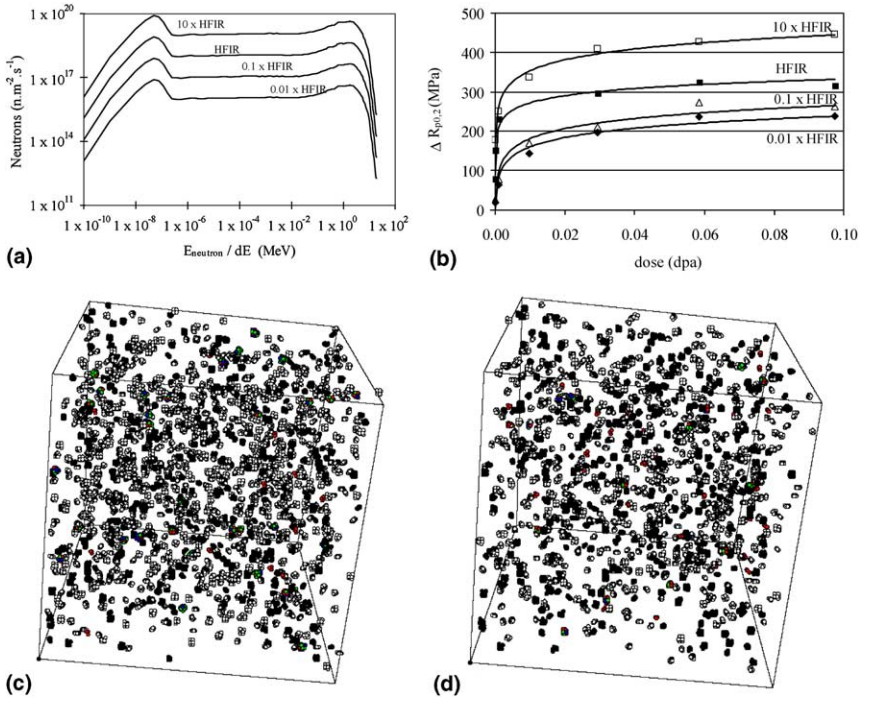

Fig. 11. Sensitivity of RPV-1 to the neutron flux. Simulations at 55 °C with one neutron spectra representative of one irradiation channel of the American experimental reactor HFIR (flux $\approx 2.6 \times 10^{19}$ n.m^{-2}s^{-1}, $E \geqslant 1$ MeV) and with three multiple spectra (steel: 0.05%Cu–1.3%Mn–0.7%Ni). (a) Neutron spectra; (b) irradiation-induced increase of yield stress; (c) distribution of hardening defects for the 10 × HFIR spectrum and a dose of 0.1 dpa; (d) distribution of hardening defects for the 0.01 × HFIR spectrum and a dose of 0.1 dpa. (Vacancy: white, SIA: black; Cu: red, Mn: green, Ni: blue; box size: $28.7 \times 28.7 \times 28.7$ nm^3.)

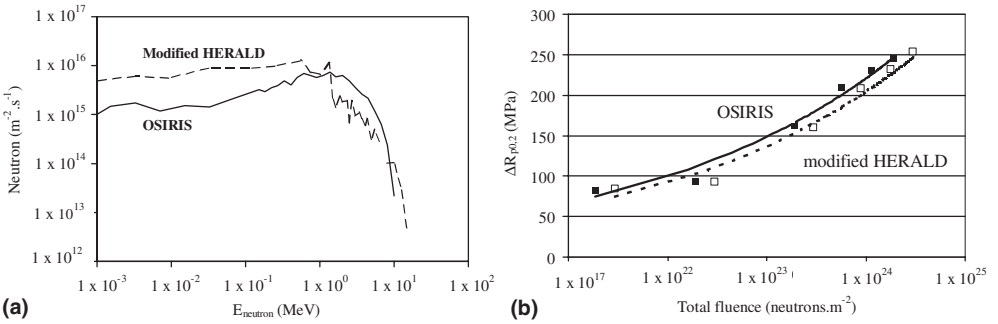

Fig. 12. Sensitivity of RPV-1 to the shape of the neutron spectrum. Simulations at 150 °C with a neutron spectrum representative of one irradiation channel of the French experimental reactor OSIRIS (flux $\approx 4.4 \times 10^{16}$ n.m^{-2}s^{-1}, $E \geqslant 1$ MeV) and one spectrum obtained by modifying a neutron spectrum representative of one irradiation channel of HERALD so as to get the same dpa rate as the OSIRIS type spectrum (steel: 0.1%Cu–1.3%Mn–0.7%Ni). (a) Neutron spectra; (b) irradiation-induced increase of yield stress; (c) distribution of hardening defects for the OSIRIS spectrum and a dose of 0.1 dpa. (d) distribution of hardening defects for the modified HERALD spectrum and a dose of 0.1 dpa. (Vacancy: white, SIA: black; Cu: red, Mn: green, Ni: blue; box size: $28.7 \times 28.7 \times 28.7$ nm^3.)

simulations were performed at 150 °C with a dose up to 0.1 dpa. A neutron spectrum representative of one irradiation channel of OSIRIS was used as reference (flux $\approx 4.4 \times 10^{16}$ n.m^{-2}s^{-1}, $E \geqslant 1$ MeV), the other one was obtained by modifying a neutron spectrum representative of an irradiation channel of HERALD so as to get the same dpa rate as the OSIRIS type spectrum (Fig. 12(a)).

The simulated irradiation-induced increases of yield stress are plotted versus the total fluence in Fig. 12.

Table 3
Some errors and uncertainties of the codes used to build RPV-1

Code	Errors and uncertainties	Impact
SPECMIN	Model errors	
	BCA approximation	Not significant in the LWR's range of neutron energies
	Neglecting of alloying elements	Not significant in the LWR's range of vessel compositions
	Lindhard model to calculate T_{damage}	Not significant in the LWR's range of PKA energies
	Dpa definition	No crucial if used to compare neutron spectra
	Numerical errors	Related to computer precision
	Programming errors	No
	Uncertainties	
	From the nuclear cross-sections	≈10% uncertainties on the results
	From neutron spectrum	Probably the main issue
INCAS	Model errors	
	BCA approximation	Not significant in the LWR's range of PKA energies
	Neglecting of alloying elements	Not significant in the LWR's range of vessel compositions
	(Sub)-cascades definition	Not crucial if used to compare neutron spectra
	Imposed distribution of point defects produced between sub-cascades	Small effect on the results
	Numerical errors	Related to computer precision
	Programming errors	Still subject of attention
	Uncertainties	
	From the collision cross-section	≈10–20% uncertainties on the results
MF-VISC	Model errors	
	Simplified capture radius	One of the main issues
	Neglecting of the interactions between copper atoms and SIAs	May be an important source of error
	Use of continuous equation for larger clusters	Probably a weak effect
	Neglecting of the multi-sink effect	May be an important source of error
	Neglecting of the mobility of vacancy-copper clusters	Probably a weak effect
	Numerical errors	Related to computer precision
	Programming errors	Still possible (young code)
	Uncertainties	
	Bad knowledge of many parameters (mobility's of clusters, binding energies,...)	One of the main issues

DIFFG	Model errors	
	Cu, Mn and Ni activities calculated from binary mixtures, within an extended regular solution model Interface energy calculated within a pair bond (nearest neighbour) regular solution model	
	Numerical errors	Related to computer precision
	Programming errors	No
	Uncertainties	
	Mixing enthalpies, entropies and free energies to describe bcc binary mixtures	Probably a weak effect
DUPAIR	Model errors	
	Tension line constant along the bowed dislocation segment	Probably a small effect when the number density of defects is high or when the obstacles are weak
	No effect of the irradiation-induced damage on the Peierls friction stress	Probably a weak effect
	No possibility of cross-slip	Probably a weak effect
	Possibility to pass of small defects by thermal activation processes	Probably a weak effect
	Simulation with only one dislocation	Probably a weak effect
	Numerical errors	Related to computer precision
	Programming errors	Still subject of attention
	Uncertainties	
	Pinning forces of the obstacles	One of the main issues
DYMOKA	Model errors	
	Neglecting of relativist effects	Probably no significant effect
	Neglecting of electron–phonon interactions	Possible effect in the simulation of displacement cascades
	Numerical errors	Related to computer precision
	Programming errors	May still contain some minor errors
	Uncertainties	
	Inter-atomic potentials	Probably the main issue
LAKIMOCA	Model errors	
	Choice of the events accounted for in OKMC	Can be mastered
	Model for migration energies of vacancies in VKMC	One of the main sources of error
	Numerical errors	Related to computer precision
	Programming errors	May still contain some minor errors
	Uncertainties	
	Frequency of occurrence of events for OKMC	One of the main issues
	Inter-atomic potentials for VKMC	One of the main issues

The two spectra induce slightly different hardening, which shows that RPV-1 is sensitive to the shape of the neutron spectrum.

5.2. Errors and uncertainties

As described in previous sections, RPV-1 relies on many hypotheses and contains errors as well as uncertainties which may alter the quantitative character of the simulations. It is noteworthy that these weaknesses are not critical for the development of VTR's. Indeed, continuous improvement of computer power, understanding of irradiation effects and use of large database of experimental results [9,86,87] will help introduce more and more precise physical descriptions of the involved phenomena in the simulation. Concerning RPV-1, Table 3 summarizes some errors (in addition to the already described homogenizations) and uncertainties in the codes used to build it. A considerable effort would be required to quantify the effects of these errors and uncertainties on the simulation results. Some rules on thumb are given in Table 3.

To assess the quantitative character of RPV-1, simulation results were compared with results of a dedicated experimental program carried out by the Nuclear Center of Mol (SCK-CEN) [9]. Experimental results provided by other partners or available in the open literature were also used. The comparison showed that most of the RPV-1 results fall within the statistical dispersion of experimental results (see one example in Fig. 9). This comparison will be given in a companion paper [12].

A first step in the improvement of RPV-1 has been started by an interative procedure consisting in (i) comparison of simulation results with the database of the IVAR experimental program [86] led by the University of California Santa Barbara (this program provides a coherent set of mechanical testing data as well quantitative microstructural information on a very large range of materials irradiated in a large range of flux, fluence and temperature) and (ii) improvement of models and parameters.

6. Conclusion

RPV-1 is made of five codes and two databases which are linked up so as to receive, treat and/or transmit data. A user friendly Python interface eases the running of the simulations and the visualization of the results. RPV-1 relies on many simplifications and approximations and has to be considered as a prototype aimed at clearing the way. Long-term efforts will be required to complete it and to build successive generations of more and more sophisticated versions. Nevertheless, RPV-1 is sensitive to its input data (neutron spectrum, temperature,...) and provides results in conformity with experimental ones. It can already be used for many applications (understanding of experimental results, assessment of effects of material and irradiation conditions,...). The iterative improvement of RPV-1 has been started by the comparison of simulation results with the database of the IVAR experimental program [86] led by the University of California Santa Barbara.

These first successes led 40 European organizations to start developing RPV-2 an advanced version of RPV-1, as well as INTERN-1, a VTR devised to simulate irradiation effects in stainless steels, in a large effort (the PERFECT project) supported by the European Commission in the framework of the 6th Framework Program.

Acknowledgment

We thank Dr C. Domain whose expertise in Computer Science and Technology was decisive in the building of RPV-1 as well as Mr. Y. Souffez (EDF) who set up the first version of the interface. We express also our gratefulness to Professor R. Odette for his kind hosting and fruitful discussions on the REVE project.

References

[1] T. De la Rubia, V.V. Bulatov, MRS Bull. 26 (2001) 169.
[2] G.R. Odette, B.D. Wirth, D.J. Bacon, N.M. Ghoniem, MRS Bull. 26 (2001) 176.
[3] G.R. Odette, Scr. Metall. 11 (1983) 1183.
[4] G.E. Lucas, G.R. Odette, P.M. Lombrozo, J.W. Sheckherd, ASTM STP 870 (1985) 900.
[5] E.D. Eason, J.E. Wrigth, G.R. Odette, Improved Corrrelations for Reactor Pressure Steels, NUREG/CR-6551, 11998.
[6] S. Jumel, RPV-1: a Virtual Reactor to Simulate Irradiation Effect in Pressurized Water Reactor Pressure Vessel steels, PhD thesis, Université de Lille (2005).
[7] S. Jumel, C. Domain, J. Ruste, J.C. Van Duysen, C. Becquart, A. Legris, P. Pareige, A. Barbu, E. Van Walle, R. Chaouadi, M. Hou, G.R. Odette, R.E. Stoller, B.D. Wirth, ASTM STP 1405 (2000).
[8] S. Jumel, C. Domain, J. Ruste, J.C. Van Duysen, C. Becquart, A. Legris, P. Pareige, A. Barbu, E. Van Walle, R. Chaouadi, M. Hou, G.R. Odette, R. Stoller, B.D. Wirth, J. Testing Evaluat. 30 (2002) 37.
[9] L. Malerba, E. Van Walle, C. Domain, S. Jumel, J.C. Van Duysen, in: Proceedings of ICONE-10: 10th International Conference on Nuclear Engineering, Arlington, USA, 2002.
[10] S. Jumel, J.C. van Duysen, J. Nucl. Mater. 328 (2004) 151.
[11] S. Jumel, J.C. Van Duysen, J. Ruste, C. Domain, J. Nucl. Mater., in press.
[12] S. Jumel, J.C. Van Duysen, J. Nucl. Mater., submitted.
[13] S. Jumel, J.C. Van Duysen, AIEA, to be submitted.
[14] G.R. Odette, G.E. Lucas, Radiat. Eff. Def. Solids 144 (1998) 189.

[15] M. Vacek, ASTM STP 909 (1986) 260.
[16] G.R. Odette, P.M. Lombrozo, Physically Based Regression Correlations of Embrittlement Data from Reactor Pressure Vessel Surveillance Programs, EPRI Report NP-3319, 1984.
[17] E.D. Eason, J.E. Wright, Improved Embrittlement Correlation for Reactor Pressure Vessel Steels, NUREG:CR-6551, US Nuclear Regulatory Commission, 1998.
[18] J.R. Hawthorne, ASTM STP 484 (1970) 96.
[19] C. Guionnet, Y. Robin, C. Flavier, A. Lefort, D. Gros, R. Perdreau, ASTM STP 725 (1981) 20.
[20] J.D. Varsik, S.T. Byrne, ASTM STP 683 (1979) 252.
[21] S. Miloudi, Etude du Dommage d'Irradiation dans les Aciers de Cuve des Réacteurs à Eau Pressurisée, PhD thesis, Université d'Orsay, 1997.
[22] J.T. Buswell, C.A. English, M.G. Hetherington, W.J. Phythian, G.D.M. Smith, G.M. Worral, ASTM STP 1046 (1990) 127.
[23] M. Akamatsu, Evolution Structurale d'Alliages Ferritiques sous Irradiation, PhD thesis,, Université d'Orsay, 1994.
[24] T. Harry, D.J. Bacon, Acta Mater. 50 (2002) 195; Acta Mater. 50 (2002) 209.
[25] P. Pareige, Etude à la Sonde Atomique de l'Evolution Microstructurale sous Irradiation d'Alliages Ferritiques Fe–Cu et d'Aciers de Cuve de Réacteurs Nucléaires, PhD thesis, Université de Rouen, 1994.
[26] F. Christien, A. Barbu, J. Nucl. Mater. 324 (2004) 90.
[27] P.J.E. Bischler, R.K. Wild, ASTM STP 1270 (1996) 260.
[28] E.A. Little, D.R. Harries, ASTM STP 457 (1969) 215.
[29] P.J. Barton, D.R. Harries, I.L. Mogford, J. Iron Steel Inst. 203 (5) (1965) 507.
[30] G.R. Odette, G.E. Lucas, ASTM STP 909 (1986) 206.
[31] J.R. Hawthorne, Nucl. Technol. 59 (3) (1982) 41.
[32] J.R. Hawthorne, ASTM STP 819 (1983) 100.
[33] C. Guionnet, B. Houssin, D. Brasseur, A. Lefort, D. Gros, R. Perdreau, ASTM STP 782 (1982) 392.
[34] G.R. Odette, Mat. Res. Soc. Symp. Proc. 373 (1995) 137.
[35] M.G. Burke, R.J. Stofanak, J.M. Hyde, C.A. English, W.L. Server, ASTM STP 1447 (2003).
[36] J.M. Hyde, D. Ellis, C.A. English, T.J. Williams, ASTM STP 1405 (2001) 262.
[37] G.R. Odette, B.D. Wirth, J. Nucl. Mater. 251 (1997) 157.
[38] P. Auger, P. Pareige, S. Welzel, J.C. Van Duysen, J. Nucl. Mater. 280 (2000) 331.
[39] M. Akamatsu, J.C. Van Duysen, P. Pareige, P. Auger, J. Nucl. Mater. 225 (1995) 192.
[40] C. Domain, C. Becquart, J.C. Van Duysen, Mat. Res. Soc. Symp. 650 (2001) R3.25.1.
[41] C.S. Becquart, C. Domain, J.C. Van Duysen, J.M. Raulot, J. Nucl. Mater. 294 (2001) 274.
[42] A.B. Lidiard, Philos. Mag. A 79 (6) (1999) 1493.
[43] S.G. Druce, C.A. English, A.J.E. Foreman, R.J. McElroy, I.A. Vatter, C.J. Bolton, J.T. Buswell, R.B. Jones, ASTM STP 1270 (1996) 119.
[44] R.G. Faulkner, D.J. Bacon, S. Song, P.E.J. Flewitt, J. Nucl. Mater. 271&272 (1990) 1.
[45] D. Meade, R.G. Faulkner, D. Ellis, ASTM STP 1366 (2000).
[46] D. McLean, Grain Boundaries in Metals, Oxford University, 1957.
[47] M. Guttmann, Surf. Sci. 53 (1975) 213.
[48] M.P. Seah, Acta Metall. 25 (1977) 345.
[49] G.R. Odette, E.V. Mader, G.E. Lucas, W.J. Phythian, C.A. English, ASTM STP 1175 (1993) 373.
[50] P. Pareige, P. Auger, J.C. Van Duysen, J. Phys. IV 11 (2001).
[51] M.K. Miller, K.F. Russell, R.E. Stoller, P. Pareige, Atom Probe Tomography Characterization of the Solute Distribution in a Neutron-irradiated and Annealed Pressure Vessel Steel Weld, Report NUREG/CR-6629, ONRL/TM-13768.
[52] J.M. Hyde, C.A. English, Microstructural Characterization of RPV Steels – Summary of Phases I&II and Next Program Plan, Report AEAT-4159, 1998.
[53] G.R. Odette, C.K. Sheeks, in: J.R. Holland, L.K. Mansur, D.I. Potter (Eds.), TMS AIME (1982) 415.
[54] C. Domain, personal communication.
[55] M.A. Puigvi, Y.N. Osetsky, A. Serra, Philos. Mag., in press.
[56] B.D. Wirth, G.R. Odette, D. Maroudas, G.E. Lucas, J. Nucl. Mater. 276 (2000) 33.
[57] E. Kuramoto, J. Nucl. Mater. 276 (2000) 143.
[58] Y. Osetsky, A. Serra, V. Priego, J. Nucl. Mater. 276 (2000) 202.
[59] A.E. Ward, S.B. Fisher, J. Nucl. Mater. 166 (1989) 227.
[60] E.A. Little, R. Bullough, M.H. Wood, Proc. Roy. Soc. Lond., A 372 (1980) 565.
[61] N. Soneda, T. Diaz de La Rubia, Philos. Mag. A 78 (1998) 995.
[62] Y.N. Osetsky, D.J. Bacon, A. Serra, B.N. Singh, Golubov, J. Nucl. Mater. 276 (2000) 65.
[63] J. Marian, B.D. Wirth, J.M. Perlado, Phys. Rev. Lett. 88 (25) (2002) 25507-1.
[64] B.D. Wirth, PhD dissertation, University of California, Santa Barbara, 1998.
[65] C.S. Becquart, C. Domain, A. Legris, J.C. Van Duysen, J. Nucl. Mater. 280 (2000) 73.
[66] H.L. Heinisch, B.N. Singh, S.I. Golubov, J. Nucl. Mater. 283–287 (2000) 737.
[67] C. Becquart, personal communication.
[68] V.G. Kapinos, Y.N. Osetsky, P.A. Platanov, J. Nucl. Mater. 170 (1990) 66.
[69] V.G. Kapinos, Y.N. Osetsky, P.A. Platanov, J. Nucl. Mater. 173 (1990) 229.
[70] Y.N. Osetsky, D.J. Bacon, A. Serra, Mater. Res. Soc. Symp. Proc. 538 (1999) 649.
[71] A.J.E. Foreman, M.J. Makin, Philos. Mag. 14 (1964) 911.
[72] M.T. Kirk, M.A.E. Natishan, M. Wagenhofer, ASTM STP 1406 (2001).
[73] L.R. Greenwood, J. Nucl. Mater. 216 (1994) 29.
[74] J. Lindhard, V. Nielsen, M. Scharff, Det Kongelige Danske Videnskaberbernes Selskab Matematisk-fysiske Meddelelser 36 (1968) 10.
[75] M.T. Robinson, I.M. Torrens, Phys. Rev. B 9 (12) (1974) 5008.
[76] A. Hardouin-Duparc, C. Moingeon, N. Smetniansky-de-Grande, A. Barbu, J. Nucl. Mater. 302 (2002) 143.
[77] V. Duwig, A. Ponçot, Note théorique et informatique du code MFVIC, EDF Report, H-I23/2003/005, 2003.

[78] V. Duwig, S. Jumel, EDF report, Note théorique et informatique du code MFVISC, 2004.
[79] C.L. Liu, G.R. Odette, B.D. Wirth, G.E. Lucas, Mater. Sci. Eng. A238 (1997) 202.
[80] S. Jumel, C. Domain, J.C. Van Duysen, DUPAIR: A Foreman and Makin-type Code to Simulate Structural Hardening, EDF Internal Report, 2004.
[81] C.S. Becquart, K.M. Decker, C. Domain, J. Ruste, Y. Souffez, J.C. Turbatte, J.C. Van Duysen, Radiat. Eff. Def. Solids 142 (1997) 9.
[82] V. Shasstry, T. Diaz de la Rubia, J. Eng. Mater. Technol. 121 (1999) 126.
[83] J.P. Hirth, J. Lothe, Theory of Dislocations, Mc Graw Hill Inc, 1968.
[84] G.R. Odette, M.Y. He, J. Nucl. Mater. (2000) 120.
[85] G.R. Odette, ASTM STP 1270 (1996) 547.
[86] G.R. Odette, T. Yamamoto, D. Klingensmith, Philos. Mag., in press.
[87] G.R. Odette, G.E. Lucas, D. Klingensmith, B.D. Wirth, D. Gragg, The Effects of Composition and Heat Treatment on Hardening and Embrittlement of Reactor Pressure Vessel Steels, NUREG/CR6778, US Nuclear Regulatory Commission, 2003.
[88] M. Ludwig, D. Farkas, D. Pedraza, S. Schmauder, Modell. Simul. Mater. Sci. Eng. 6 (1998) 19.
[89] J.M. Raulot, Master of Science Thesis, Université de Marne la Vallée, 1998.